Three-Pulse Echo Peak Shift Studies of Polar Solvation Dynamics

Sean A. Passino, Yutaka Nagasawa, Taiha Joo,† and Graham R. Fleming*

Department of Chemistry and the James Franck Institute, The University of Chicago, Chicago, Illinois 60637

Received: July 16, 1996; In Final Form: October 4, 1996[⊗]

The three-pulse photon echo peak shift technique is used to study room temperature solvation dynamics in acetonitrile, benzonitrile, methanol, ethanol, ethylene glycol, and chloroform utilizing the tricarbocyanine dye, IR144 as the probe molecule. In all cases, an ultrafast component, ascribed to inertial solvent motion, was evident after the very rapid dephasing of the intramolecular vibrational modes. All the solvents except acetonitrile show biexponential behavior on the picosecond (diffusive) time scale. In the case of acetonitrile, the spectral density governing the solute−solvent interaction is recovered by numerical fitting of peak shift data. The inertial component of the spectral density is compared with the solvation spectral density obtained from an instantaneous normal mode calculation. The two spectra agree well. The fitting parameters allow the absorption spectrum to be well reproduced. For ethylene glycol, data are also presented for 397 K; the ultrafast component of solvation is quite independent of temperature, while the diffusive portion speeds up dramatically at high temperature.

Introduction

Experimental characterization of the strengths and time scales of the coupling of electronic transitions to their associated nuclear degrees of freedom raises the prospect of sophisticated quantum dynamical modeling of a wide variety of condensed phase chemical and biological phenomena.[1−7] The nuclear degrees of freedom just mentioned may be intramolecular (vibrational) or intermolecular in origin. Fluorescence Stokes shift measurements are mostly sensitive to the intermolecular contribution, i.e., the solvation dynamics.[8−16] Photon echo measurements are sensitive to both contributions, at least in part because they are generally conducted with much shorter excitation pulses than the fluorescence studies. A wide range of different types of photon echo measurements with varying sensitivities to all aspects of the dynamics have recently been described.[17−32] Joo[21,22] and de Boeij et al.[18] have recently shown that a form of the three-pulse stimulated photon echo, referred to as three-pulse photon echo peak shift (3PEPS), is sensitive to system−bath coupling over a wide dynamic range. In addition, the 3PEPS measurement can reveal the presence of time scales much longer than the experimental observation window (≤10 ns, a reasonable ground state recovery time for a chromophore in solution), i.e., the presence of "static inhomogeneous broadening" to which fluorescence measurements are insensitive.[17]

In parallel with the experimental developments, significant advances in theoretical descriptions of solvation phenomena and the associated line broadening have been made.[33−38] General expressions relating the experimental observable to models in which the electronic transition is coupled to a set of displaced harmonic oscillators or to one or more Brownian oscillators have been developed.[7,17,19,39−47] Descriptions of the short-time aspects of liquid dynamics based on the coupling of instantaneous normal modes (INMs) to the observable of interest have been developed.[33,34,36,39,41,48−50] For example, in the case of solvation dynamics the coupling constant weighted INM spectrum is referred to as the solvation spectral density[33,41] and reveals the dominance of rotational-type motions in polar solvation dynamics.[33,34,39,41] An attractive feature of the INM approach is that it may allow molecular identification of the harmonic oscillators used to describe the linear and nonlinear spectroscopy. Thus, for a particular solvent, a comparison of the spectral density obtained from analysis of photon echo experiments with that calculated from the INM model is of interest.

In this paper we present 3PEPS data for six different solvents obtained using the dye IR144[51] as the probe. By combining data from transient grating[22] and resonance Raman experiments,[52] we are able to describe both intramolecular and solvation contributions to the 3PEPS signal and hence to spectral line broadening. Numerical fitting of the 3PEPS data enables us to derive an experimental spectral density for S_0-S_1 absorption process of IR144 in acetonitrile. This is compared with the solvation spectral density calculated by Ladanyi and Stratt[41] for acetonitrile based on an INM model.

Theoretical Background

The basis of the 3PEPS experiment has been described in detail elsewhere,[18,19,22−24] and only a brief sketch of the background will be given here. The key quantity involved is the system bath coupling potential $V_{SB}(\{q_\alpha\},Q)$, which is a function of both bath ($\{q_\alpha\}$) and system (Q) coordinates. We partition V_{SB} into an average component and a fluctuating component

$$\delta V_{SB}(t) = V_{SB}(t) - \langle V_{SB} \rangle \tag{1}$$

Now, both linear and nonlinear spectroscopies are calculated from the line broadening function defined by

$$g(t) = \frac{1}{\hbar^2}\int_0^t d\tau \int_0^\tau d\tau' \langle \delta V_{SB}(\tau') \, \delta V_{SB}(0)\rangle \tag{2}$$

where $\delta V_{SB}(t)$ is the Heisenberg operator of δV_{SB} at high temperature. For example, the absorption spectrum profile is given by

$$\sigma_A(\omega) \propto \int_{-\infty}^{\infty} dt \exp[-i(\omega - \omega_{eg})t] \exp[-g(t)] \tag{3}$$

* Corresponding author. e-mail address: fleming@rainbow.uchicago.edu.
† Present address: Department of Chemistry, Pohang University of Science and Technology, Pohang, 790-784, Korea.
⊗ Abstract published in *Advance ACS Abstracts,* December 15, 1996.

S1089-5639(96)02138-X CCC: $14.00

and the third-order nonlinear spectroscopies calculated via the response functions R_1-R_8.[22,40] Two equivalent models for the coupling potential operators have been used: the Brownian oscillator model[40] and the harmonic bath model.[7,19,42−47] In any case, a spectral density representation can be used to represent an arbitrary bath model.[17] In other words, all the strengths and time scales of the system−bath interaction are contained in the function $\rho(\omega)$. A key purpose of this work was to obtain $\rho(\omega)$ directly from the echo measurements and to compare it with, for example, the $\rho_{solv}(\omega)$ obtained from the instantaneous normal mode model. In terms of the spectral density, the line shape function is

$$g(t) = -\frac{i\lambda t}{\hbar} + \int_0^\infty d\omega\ \rho(\omega)\coth(\hbar\beta\omega/2)(1-\cos\omega t) + i\int_0^\infty d\omega\ \rho(\omega)\sin\omega t \quad (4)$$

where λ is the reorganization energy defined as the first moment of the spectral density

$$\lambda = \hbar\int_0^\infty d\omega\ \omega\rho(\omega) \quad (5)$$

and $\beta = 1/k_BT$.

Echo signals are most often discussed in terms of the Bohr frequency correlation function, $M(t)$, defined as

$$M(t) = \frac{\langle\Delta\omega(t)\,\Delta\omega(0)\rangle}{\langle\Delta\omega^2\rangle} = \frac{1}{\langle\Delta\omega^2\rangle}\int_0^\infty d\omega\ \omega^2\rho(\omega)\times \coth\left(\frac{\hbar\beta\omega}{2}\right)\cos\omega t \quad (6)$$

where $<\Delta\omega^2>$, the mean-square fluctuation amplitude, is commonly referred to as the coupling strength.

$$\langle\Delta\omega^2\rangle = \int_0^\infty d\omega\ \omega^2\rho(\omega)\coth\left(\frac{\hbar\beta\omega}{2}\right) \quad (7)$$

Fluorescence Stokes shift studies are characterized by the Stokes shift function $S(t)$ defined as

$$S(t) = \frac{\Delta\bar{E}(t) - \Delta\bar{E}(\infty)}{\Delta\bar{E}(0) - \Delta\bar{E}(\infty)} \quad (8)$$

where $\Delta\bar{E}(t)$ is the nonequilibrium energy difference between ground and excited states. In terms of the spectral density, $S(t)$ corresponds to the time dependence of the first moment (i.e., the time-dependent reorganization energy):

$$S(t) = (\hbar/\lambda)\int_0^\infty d\omega\ \omega\rho(\omega)\cos\omega t \quad (9)$$

Note that (6) and (9) are equivalent in the high-temperature limit.

Experimental Methods

The laser system and experimental arrangement for the three-pulse echo measurements have been described previously.[21] The Kerr lens mode-locked Ti:sapphire laser operates at a center wavelength of 780 nm and for the studies described here generates 22 fs pulses with a time bandwidth product of 0.42. A pair of Brewster angle LAKL-21 prisms precompensates for the group velocity dispersion acquired from the optics between laser and sample. The compensated output was split into three roughly equal intensity rectilinear beams with parallel polarization and aligned in an equilateral triangle with each side about 8 mm, as shown in Figure 1. A 10 cm singlet lens focused the beams onto the sample. The time-reversed image 3PE signals

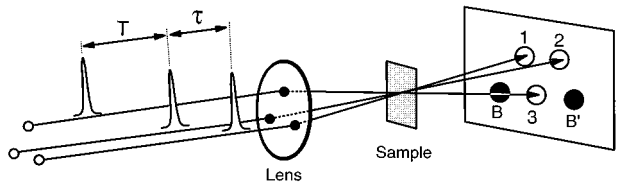

Figure 1. Experimental beam geometry and the delay periods between pulse interactions for the three-pulse echo peak shift measurements. The 3PE signal occurs at B and B′ in this geometry. Pulse interactions may occur at any point during the electric field envelope of the pulse, not necessarily at its maximum as shown. This is accounted for in the numerical simulations (vide infra).

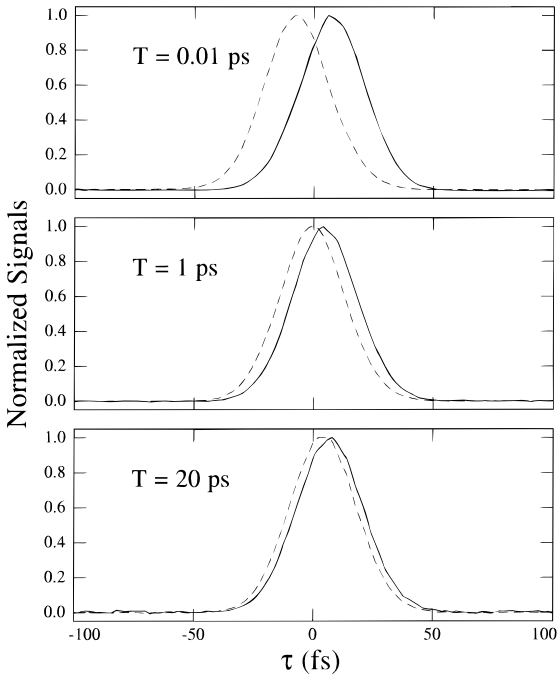

Figure 2. Integrated 3PE signals for IR144 in benzonitrile at room temperature for the following population periods: $T = 0.01$, 1, and 20 ps. For relatively small population periods, the echo signals are well separated, indicating that the system preserved its ability to rephase. At longer population periods, the echo signals are almost overlapped in time, indicating that the system has lost most of its rephasing ability.

are detected simultaneously in the two phase matched directions $\mathbf{k}_1 - \mathbf{k}_2 + \mathbf{k}_3$ and $-\mathbf{k}_1 + \mathbf{k}_2 + \mathbf{k}_3$ (shown as B and B′ in Figure 1). Here the subscripts refer to the three pulses in Figure 1. The third beam was mechanically chopped and the reference fed to two separate lock-in amplifiers. The signals at $\mathbf{k}_1 - \mathbf{k}_2 + \mathbf{k}_3$ and $-\mathbf{k}_1 + \mathbf{k}_2 + \mathbf{k}_3$ were spatially filtered, imaged onto separate 10 ns rise-time photodiodes, and input to the two lock-in amplifiers whose simultaneously monitored outputs were fed to an A/D board and subsequently processed by our data collection software.

Figure 1 also indicates the time intervals between the pulses. Pulses 1 and 2 are separated by τ, while pulses 2 and 3 are separated by T, which we refer to as the population period since during this interval the system propagates in a diagonal (ground or excited) state. The integrated echo intensity over the period $t = -\infty$ to ∞ is detected. Typical integrated 3PE signals for three different population periods are shown in Figure 2 for IR144 in benzonitrile, with the solid and dashed curves representing the signals detected at positions B′ and B, respectively. The integrated echo signals are quite symmetric and were fit to Gaussian functions. Half the separation of the center of the two fitted Gaussians accurately specifies the delay of the echo signal from zero delay on the τ axis. This quantity, $\tau^*(T)$, is the primary variable of interest here; measurement of

τ^* for a series of different values of T, the population period, contributes what we have called a 3PEPS measurement. The experimental reproducibility of peak shift values is ±0.3 fs. About 80 sets of τ scans for differing values of T are used to construct a typical 3PEPS data set. The maximum value of T was typically 300−500 ps.

In systems with no static inhomogeneity, we expect the long time value of τ^*, $\tau^*(\infty)$, to be zero.[17] However, use of the 10 cm singlet focusing lens results in a small (∼1.5 fs) value of $\tau^*(T)$ at large values of T where the signal is constant. Using a 20 cm achromat lens reduces τ^* (∞) to zero, suggesting that the finite asymptotic value is an artifact and results from chromatic aberration and/or the larger crossing angle in the 10 cm case.[20] All of the data discussed here were collected with a 10 cm singlet lens, and the constant long time value was subtracted from each individual $\tau^*(T)$ vs T curve to make the final value zero, as is expected for systems with no dynamical time scales longer than a few tens of picoseconds.[17]

The IR144 (Exciton) and acetonitrile, benzonitrile, chloroform, methanol, ethanol, and ethylene glycol (Aldrich Chemical Co.) were used as received. Experiments were conducted at ambient temperatures of approximately 297 K (unless otherwise noted) with a peak sample OD of approximately 1, as determined by an absorption spectra obtained from a Shimadzu UV-1601 UV−vis spectrophotometer.

The sample was circulated at about 1 mL/s through a 0.1 mm quartz flow cell. The pulse energy before the antireflection-coated lens never exceeded 200 pJ in each beam to avoid thermal gratings and higher order signals.[22,53,54] The repetition rate of the laser was varied between 20 and 253 kHz; this did not affect the echo signals.

Results

From sets of measurements of the type shown in Figure 2, the peak shift ($\tau^*(T)$) is constructed as a function of T. Figure 3 shows typical 3PEPS data for IR144 in ethanol, ethylene glycol, benzonitrile, and chloroform, on two distinct time scales. Similar data were collected for acetonitrile and methanol. In all cases the peak shift decreases by ∼75% in the first 200 fs. Weak oscillations (clearly evident at 193 fs) result from intramolecular vibrational modes. On the picosecond time scale, where the peak shift corresponds directly to the solvation dynamics, the differences between the four solvents become strikingly clear.

For an initial analysis of the data, we fit the peak shift data to sums of exponentials. As discussed elsewhere, this procedure gives time constants directly related to the solvation correlation function for times longer than the bath correlation time (∼100−200 fs).[17] The shortest time scales do not directly correspond to time scales in the underlying correlation function and appear exponential in the peak shift curve even if they are, for example, Gaussian in $S(t)$.[22] Table 1 presents fits to the peak shift data for the six solvents. There are clearly three phases in the decay of $\tau^*(T)$ in all cases: (1) an initial very rapid decay arising from intramolecular vibrations (vide infra) giving a component of ∼ 6 fs; (2) an ∼60 fs component which we believe arises mainly from the inertial component of solvation; (3) picosecond time scale components that vary significantly from solvent to solvent. In all cases except acetonitrile, this relaxation can be resolved into two exponential decays. Since intramolecular vibrational contributions to the dynamics are generally not observed in fluorescence Stokes shift studies, to facilitate comparison with these studies Table 2 presents exponential fits to the peak shift data with the 6 fs component removed. Following the discussion of Joo et al.,[22] we note that the amplitude of the inertial component is overestimated and its time constant underestimated by exponential fits of $\tau^*(T)$ vs T. τ_2 and τ_3 in Table 2 and their relative amplitudes should be directly comparable to, for example, the results of Horng et al.[10] Overall, the level of agreement is good—small differences may well result from the different probes employed. One difference that should be mentioned, however, is that in most of the solvents studied here Horng et al.[10] recover a component of 200−300 fs in their fits of $S(t)$. We do not find such a

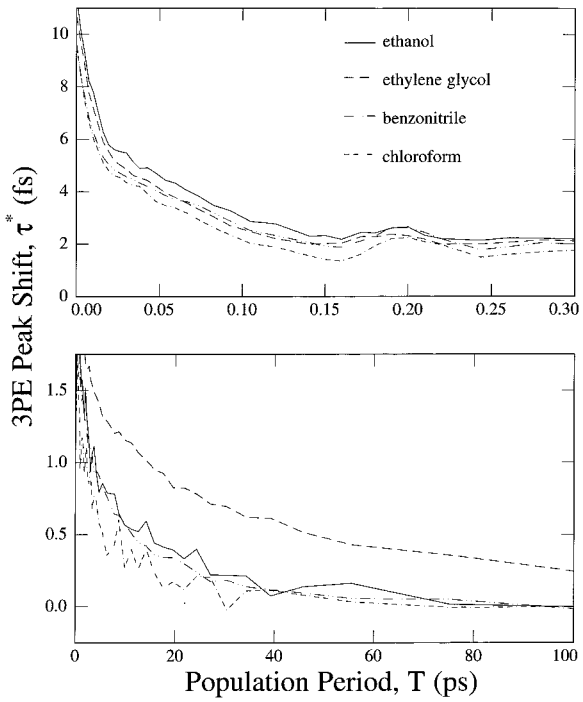

Figure 3. Three-pulse echo peak shift data for IR144 in the following solvents: ethanol, ethylene glycol, benzonitrile, and chloroform at 297 K. These data clearly resolve rapid incipient dynamics, quantum beats (at 193 fs) (upper panel, 0−0.3 ps), and "slower" diffusive solvation dynamics (lower panel, 0−100 ps). Note the presence of slow relaxation in ethylene glycol.

TABLE 1: Nonlinear Least-Squares Fitting Results for the 3PE Peak Shift Data, $\tau^*(T)$ vs T[a]

solvent	a_1	τ_1	a_2	τ_2	a_3	τ_3	a_4	τ_4
acetonitrile	0.316	0.0065	0.567	0.073	0.128	2.23		
benzonitrile	0.339	0.0062	0.437	0.060	0.105	1.64	0.119	14.6
chloroform	0.313	0.0056	0.487	0.050	0.102	1.40	0.099	11.4
ethylene glycol	0.348	0.0071	0.454	0.050	0.078	4.04	0.119	53.7
ethylene glycol[b]	0.410	0.0060	0.372	0.057	0.129	1.36	0.088	16.2
ethanol	0.334	0.0070	0.455	0.062	0.106	2.03	0.105	19.9
methanol	0.310	0.0078	0.503	0.062	0.114	1.47	0.073	9.47

[a] The fitting function is the sum of four exponentials (three for acetonitrile) with amplitudes a_i and inverse decay rates τ_i (in picoseconds). The amplitudes are normalized. [b] Solvent at 397 K. All other solvents are at ambient temperature of approximately 297 K.

TABLE 2: Peak Shift Fits Excluding the Fastest Decaying Component in Table 1

solvent	a_2	τ_2	a_3	τ_3	a_4	τ_4
acetonitrile	0.813	0.073	0.187	2.23		
benzonitrile	0.661	0.060	0.159	1.64	0.180	14.6
chloroform	0.709	0.050	0.148	1.40	0.143	11.4
ethylene glycol	0.698	0.050	0.120	4.04	0.183	53.7
ethylene glycol[a]	0.633	0.057	0.217	1.36	0.150	16.2
ethanol	0.683	0.062	0.160	2.03	0.157	19.9
methanol	0.729	0.062	0.167	1.47	0.104	9.47

[a] Solvent at 397 K. All other solvents are at ambient temperature of approximately 297 K. Inverse decay rates in picoseconds.

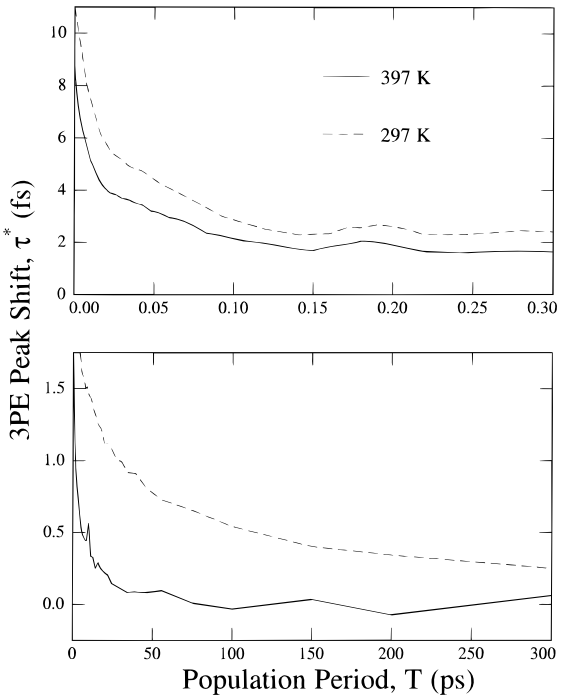

Figure 4. Influence of temperature on 3PEPS for IR144 in ethylene glycol. Data at 297 and 397 K are shown. The fastest phases of relaxation (upper panel, 0−0.3 ps) decay almost at the same rate for both temperatures. The picosecond components (lower panel, 0−300 ps) are dramatically affected by temperature: relaxation is incomplete even at $T > 300$ ps at ambient temperature, but at 397 K it is complete by about 50 ps (Table 1).

component in our peak shift fits and numerical simulations of peak shift data using Horng et al.'s parameters for $S(t)$ ($=M(t)$) suggest that we would find it if it were present. We do not know the reason for this discrepancy between the fluorescence and echo fits.

We have also investigated the temperature dependence of $\tau^*(T)$ in several solvents. The largest range covered was in ethylene glycol, and Figure 4 and Tables 1 and 2 show results at 397 K compared to 297 K. The upper panel of Figure 4 shows that the two fast phases of the relaxation are essentially independent of temperature over this range. The decrease in the initial value of the peak shift at high temperature presumably reflects the increase in amplitude of the fluctuations ($\langle\Delta\omega^2\rangle$).

The temperature independence of the inertial solvation component is in accord with our assumption that 297 K is already in the high-temperature limit for the solvation spectral density. We illustrate this in more detail below for acetonitrile. As the lower panel of Figure 4 shows, the effect of temperature on the picosecond components is dramatic for ethylene glycol. Both τ_2 and τ_3 components decrease by almost a factor of 4, and while relaxation is still occurring at 300 ps at 297 K, by ~50 ps ethylene glycol at 397 K is effectively homogeneous.

Numerical Fitting of the Peak Shift and Obtaining the Spectral Density for IR144 in Acetonitrile. The intramolecular contribution to the signal adds significantly to the complexity of fitting the entire time dependence of $\tau^*(T)$. In order to contain the fitting procedure, it is necessary to determine the frequencies and damping times of the intramolecular modes separately.

Our strategy is to write the Bohr frequency correlation function, $M(t)$, as a sum of four terms, matching the four time scales in the peak shift (cf. Table 1)

$$M(t) = a_{\text{gau}} \exp\left(-4 \ln 2\left(\frac{t}{\tau_{\text{gau}}}\right)^2\right) + \sum_{j=1}^{2} a_j \exp(-t/\tau_j) + \sum_{i=1}^{12} a_i \exp(-t/\gamma_i) \cos(\omega_i t + \phi_i) \quad (10)$$

The inertial component of solvation was introduced as a simple Gaussian component ($\tau_{\text{gau}} = 190$ fs for acetonitrile) while the diffusive components were treated as one ($\tau_1 = 2.23$ ps for acetonitrile) or two (all other solvents in Tables 1 and 2) exponentials. This model appeared adequate for all the systems studied. We obtained the vibrational frequencies and their damping times from our previous fit of transient grating data for IR144 in ethanol.[22] The transient grating signal of IR144 in acetonitrile (not shown) reveals no major differences from the signal in ethanol. In addition, we added two high-frequency modes observed in the resonance Raman spectrum of IR144.[52] Also required are the individual coupling strengths and the total reorganization energy so that both the 3PEPS data and the absorption spectrum can be reproduced. The total reorganization energy was constrained to be 1500 cm^{-1}; as will be seen, this produces a good description of the absorption profile. For the intramolecular vibrational modes we used the multimode Brownian oscillator (MBO) model[40] to obtain coupling strengths via

$$\langle\Delta\omega_i^2\rangle = (2\lambda_i\omega_i/\hbar)[\bar{n}_i + {}^1/_2] \quad (11)$$

where

$$\bar{n}_i = \frac{1}{\exp(\beta\hbar\omega_i) - 1} \quad (12)$$

is the thermal occupation number. The set of vibrations, their damping times, and reorganization energies are given in Table 3. Except for the two highest frequency modes, the relative reorganization energies were obtained directly from experimental transient grating measurements; the reorganization energies of the two highest frequency modes were obtained from numerical simulations of the absorption spectra. The phases of these modes were found by numerical simulations of the peak shift.

Subsequently, the total reorganization energy of the vibrational modes was subtracted from the total reorganization energy, and what remains was partitioned to the inertial (62% for acetonitrile) and dielectric components. Again, the high-temperature limit applies, and we obtained the coupling constants from the reorganization energies of these components by

$$\langle\Delta\omega^2\rangle = 2\lambda k_B T/\hbar^2 \quad (13)$$

Parameter optimization was obtained by numerical simulations of our 3PE data using our model $M(t)$, coupling strengths, and reorganization energies as inputs. The simulation procedure which includes all possible time orderings of the pulse interactions, and propagation on both ground and excited states[22,40] has been described at length elsewhere.[22]

Figure 5 shows the total Bohr frequency correlation function, $M(t)$, weighted by the coupling strengths: i.e., the amplitude coefficients in eq 10 equal the coupling strengths of its component. Also shown individually are the vibrational (without the two highest frequency modes) and inertial contributions. The lower panel shows the spectral density obtained via eq 6. With exception of the lowest frequency peak, all the spectral sharp structure in $\rho(\omega)$ arises from the intramolecular

TABLE 3: Input Parameters for the 3PEPS Simulation[a]

ω (cm^{-1})	λ (cm^{-1})	γ (fs)	ϕ (rad)
85	4.83	630	0.32
138	25.4	320	0.45
204	3.39	500	0.96
302	5.47	890	0.42
317	63.4	110	0.16
437	3.75	1000	0.88
479	9.07	260	−0.10
571	4.57	580	2.90
645	0.323	1600	2.55
709	0.346	1800	1.51
1159	139	1500	0.12
1625	293	1500	2.78

[a] Frequencies (ω), reorganization energy (λ), damping times (γ), and phases (ϕ) used for the 3PEPS simulation of IR144 in acetonitrile. See eq 10.

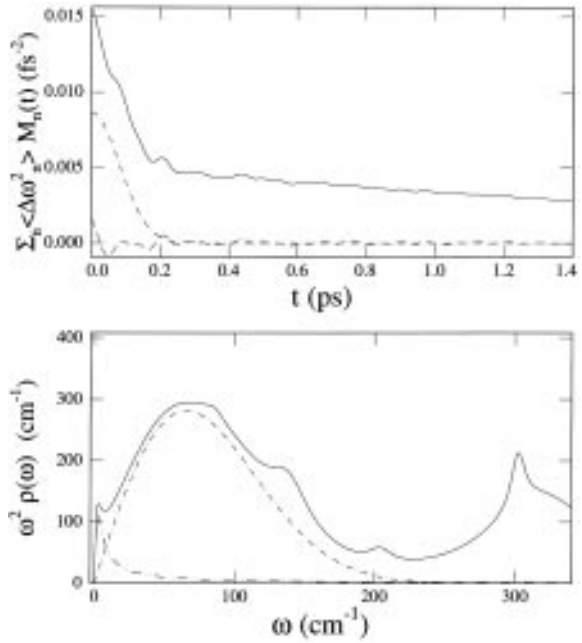

Figure 5. (upper panel) The Bohr transition frequency correlation function weighted by total coupling strength, $\sum_n \langle \Delta\omega^2_n \rangle M_n(t)$, is shown (solid line) with the individual contributions from the inertial (− · −) and oscillatory (− −) components. Note that we exclude the two highest frequency oscillations. The spectral density calculated from eq 6 (solid line, lower panel) is also shown. In addition, the inertial (− · −) and diffusive components (− ·· −) of the spectral density are shown individually.

vibrations. The lowest frequency peak is the diffusive contribution from the picosecond solvation component. The broad peak centered at 66 cm^{-1} represents the librational contribution. Both librational and diffusive components are shown separately in the figure. The librational peak strongly resembles the Ohmic form seen in optical Kerr studies[14,27,55,56] and in INM calculations.[33,34,36,41,48−50] The diffusive peak occurs at about 2.5 cm^{-1} and is clearly separable from the librational peak. This clear separation in the time scales suggests that the diffusive component will appear as a well-defined "inhomogeneous" contribution for processes faster than 1 ps in acetonitrile. The sharpness of this peak is in part related to the fact that acetonitrile possesses a single dielectric time scale, unlike the other solvents in Tables 1 and 2. Finally, we note that the diffusive component in acetonitrile has the smallest relative coupling strength of the solvents studied.

Figure 6 shows the calculated and experimental 3PEPS signals for IR144 in acetonitrile. A 22 fs Gaussian pulse was used for the calculation. The peak shift is not well fit up to 15−20 fs,

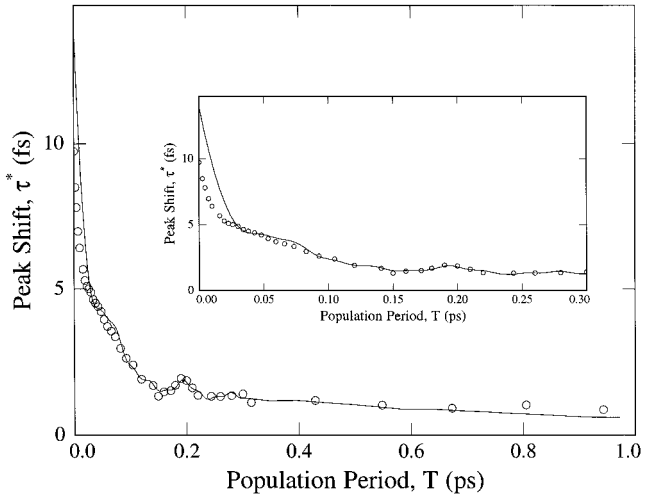

Figure 6. Comparison of calculated (—) and experimental (○) 3PEPS data for IR144 in acetonitrile at 297 K, using the $M(t)$ from Figure 5.

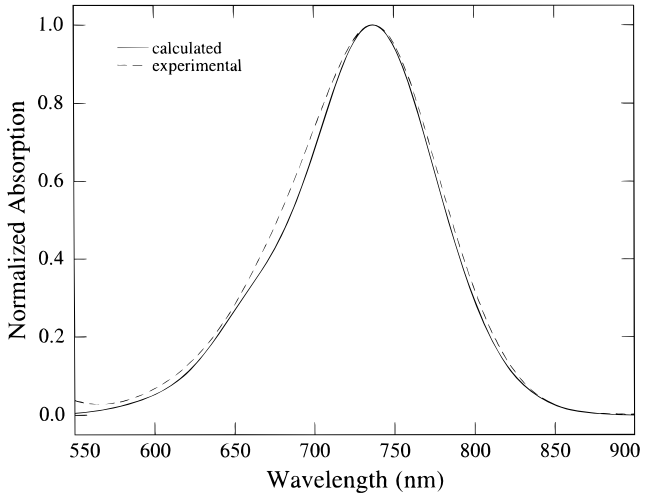

Figure 7. Calculated (—) and measured (− −) absorption spectra for IR144 in acetonitrile.

but after that the fit is excellent. As the inset shows, the fit in the region dominated by the inertial solvation dynamics (20−200 fs) is good, giving confidence that this component, as well as the diffusive contributions, is well determined. What may not be perfectly determined is the contributions (and phases) of the intramolecular modes, particularly the higher frequency modes. However, Figure 7 shows the absorption spectrum of IR144 in acetonitrile is quite well described using the parameters from Figure 6, and we believe that the full spectral density (intra- plus intermolecular contributions) is well determined for frequencies below ∼350 cm^{-1} (Figure 5). Note that since the phases of the oscillations listed in Table 3 arise from the multiple pulse interactions, the linear absorption profile contains no phase information. Therefore, all phases in Table 3 were set to zero for this calculation.

We examined the sensitivity of our calculated 3PEPS results by seeing how the Gaussian frequency changes when we varied the contribution from the intramolecular modes. The solvation frequency[10] changes from 71 to 66 cm^{-1} depending upon whether we used the first eight modes in Table 3 or all 10, respectively. Varying the phases and coupling strengths (within the constraints imposed by the absorption spectrum) of these modes does not move the Gaussian frequency out of the above range.

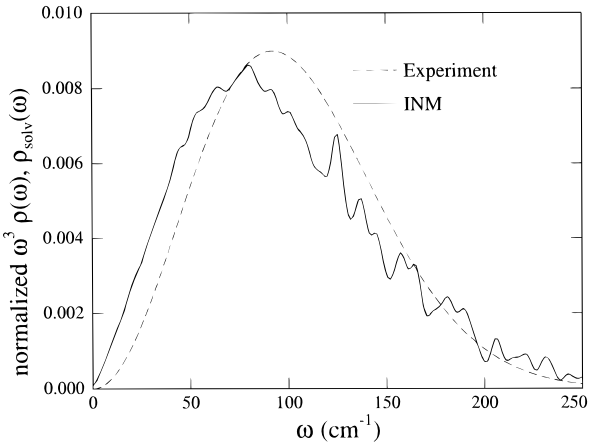

Figure 8. Comparison of the instantaneous normal mode solvation spectrum of acetonitrile calculated by Ladanyi and Stratt[41] ($\rho_{solv}(\omega)$ is the solid line) and the rescaled (see text) spectral density from Figure 5 ($\omega^3\rho(\omega)$ is the dashed line). Only the inertial portion of the spectral density in Figure 5 was used. Both curves were normalized in the region 0−340 cm^{-1} for comparison. This removes the contribution from the imaginary INMs.

Discussion

Solvation dynamics in acetonitrile have been extensively studied by fluorescence Stokes shift experiments,[8−16] photon echoes,[17−32] computer simulations,[57−60] analytical theory,[14,33−35,37,38] and the INM model.[33,34,36,39,41,48−50] A consensus view is that librational motion is the dominant mechanism for solvation in this solvent. This is shown, for example, by the molecular dynamics simulations of Maroncelli[59,60] and the INM approach of Ladanyi and Stratt,[39,41] who showed that the shape of the solvation spectrum, $\rho_{solv}(\omega)$, derived for acetonitrile strongly resembles the rotational contribution to the INM spectrum itself.[41] The solvation spectrum is derived by weighting the basic INM spectrum with the squares of the coupling constants, c_α, defined with respect to the INM coordinates, q_α, via

$$c_\alpha = \partial \Delta E / \partial q_\alpha \qquad (14)$$

where ΔE is the solute−solvent energy. The definition of $\rho_{solv}(\omega)$ by Ladanyi and Stratt[61] differs from our $\rho(\omega)$ in Figure 5 by a factor of ω^3. In order to compare the experimental and calculated spectra, we compare the rescaled $\rho(\omega)$ from Figure 5 with $\rho_{solv}(\omega)$ of Ladanyi and Stratt[41] in Figure 8. Only the librational peak is included in the experimental spectrum. The two spectra are normalized over the range 0−340 cm^{-1}: i.e., the imaginary INM modes are neglected. The general shapes are extremely similar although the INM spectrum peaks at a lower frequency (75−80 cm^{-1}) than the experimental one (93 cm^{-1}). The striking similarity of the two curves in Figure 8 gives confidence that INM approaches should accurately describe short-time dynamics in liquids. Of course, the INM approach, being based on harmonic modes, fails to capture the diffusive spike in the full spectral density (Figure 5).

This comparison seems to bring full circle the proposal of Cho et al. that the spectral density obtained from optical Kerr studies, $\rho_{pol}(\omega)$, could be used to model solvation dynamics.[14] They tested their proposal against experimental Stokes shift data for LDS750 in acetonitrile with good results.[15] Scherer and co-workers extended this approach and used it in the analysis of a series of echo measurements in a variety of solvents.[27] In general, one might expect the spectrum of couplings (the c_α in eq 14) to vary significantly for different observables such as the solvation and polarizability. Thus, it is not obvious that the $\rho_{solv}(\omega)$ and $\rho_{pol}(\omega)$ should be identical. Ladanyi and Klein have investigated this point from the INM perspective in acetonitrile[48] and found that the polarizability spectrum $\rho_{pol}(\omega)$, is extraordinarily similar to $\rho_{solv}(\omega)$. Both spectra resemble the rotational INM spectrum, but are shifted to slightly higher frequencies and have a smaller contribution from imaginary modes than the INM rotational spectrum.[41,48] As noted by Ladanyi and Klein, this latter difference arises from the fact that much of $\rho_{solv}(\omega)$ arises from first-shell solvent molecules whereas much of $\rho_{pol}(\omega)$ arises from single molecular polarizabilities which are independent of intermolecular separations.[48] Of course, it remains to be seen how far this remarkable correspondence between $\rho_{solv}(\omega)$ and $\rho_{pol}(\omega)$ can be extended to other solvents, but, except in cases of high symmetry (e.g., the nearly spherical polarizability tensor of water), a reasonable similarity between the two spectra should hold. The comments of Lund et al.[62] regarding the similarity of far-infrared absorption and depolarized Rayleigh wing scattering of symmetric top molecules are of interest in this context.

Concluding Remarks

The three-pulse echo peak shift technique is shown to be sensitive to the interaction of electronic and nuclear degrees of freedom over a wide range of time scales. On the picosecond time scale, the diffusive portion of solvation dynamics is revealed directly in the peak shift data. Accurate extraction of the short-time portion of the solvation dynamics requires careful numerical analysis, both on account of the intramolecular vibrational contribution to the signal and because the underlying correlation function must be extracted from the peak shift data by numerical fitting using finite−temporal duration optical fields. Such an analysis for acetonitrile yields a spectral density for the electronic transition under study (S_0-S_1, in IR144) in close accord with that used previously to model the solvation dynamics in acetonitrile.[27,59,60] The spectral density is also very similar to the solvation spectral density calculated for acetonitrile by Ladanyi and Stratt from an instantaneous normal mode perspective,[41] giving confidence in the ability of this latter approach to model short-time dynamics in liquids.

Acknowledgment. We thank Prof. Terry Gustafson and Dr. M. Vitale for measurements of the resonance Raman spectrum of IR144. We thank Profs. Branka Ladanyi and Richard M. Stratt for providing the INM spectrum in Figure 8 and a preprint of ref 41. This work was supported by the NSF; T.J. and Y.N. were supported in part by donors to the ACS−Petroleum Research Fund and Y.N. also by JSPS and S.A.P. by a GAANN Fellowship.

References and Notes

(1) Makri, N.; Sim, E.; Makarov, D. E.; Topaler, M. *Proc. Natl. Acad. Sci. U.S.A.* **1996**, *93*, 3926−3931.
(2) Cho, M.; Silbey, R. J. *J. Chem. Phys.* **1995**, *103*, 595−606.
(3) Egger, R.; Mak, C. H. *J. Phys. Chem.* **1994**, *98*, 9903−9918.
(4) Song, X.-Y.; Marcus, R. A. *J. Chem. Phys.* **1993**, 7768−7773.
(5) Bader, J. S.; Kuharski, R. A.; Chandler, D. *J. Chem. Phys.* **1990**, *93*, 230−236.
(6) Creighton, S.; Hwang, J.-K.; Warshel, A.; Parson, W. W.; Norris, J. *Biochemistry* **1988**, *27*, 774−781.
(7) Garg, A.; Onuchic, J. N.; Ambegoakar, V. *J. Chem. Phys.* **1985**, *83*, 4491−4503.
(8) Bingemann, D.; Ernsting, N. P. *J. Chem. Phys.* **1995**, *102*, 2691−2700.
(9) Gustavsson, T.; Baldacchino, G.; Mialocq, J.-C.; Pommeret, S. *Chem. Phys. Lett.* **1995**, *236*, 587−594.
(10) Horng, M. L.; Gardecki, A.; Papuzayan, A.; Maroncelli, M. *J. Phys. Chem.* **1995**, *99*, 17311−17337.
(11) Jimenez, R.; Fleming, G. R.; Kumar, P. V.; Maroncelli, M. *Nature* **1994**, *369*, 471−473.

(12) Rosenthal, S. J.; Jimenez, R.; Fleming, G. R.; Kumar, P. V.; Maroncelli, M. *J. Mol. Liq.* **1994**, *60*, 25−56.
(13) Easter, D. C.; Baronavski, A. P. *Chem. Phys. Lett.* **1993**, *201*, 153−158.
(14) Cho, M.; Rosenthal, S. J.; Scherer, N. F.; Ziegler, L. D. *J. Chem. Phys.* **1992**, *96*, 5033−5038.
(15) Rosenthal, S. J.; Xie, X. L.; Du, M.; Fleming, G. R. *J. Chem. Phys.* **1991**, *95*, 4715−4718.
(16) Barbara, P. F.; Jarzeba, W. *Adv. Photochem.* **1990**, *15*, 1−68.
(17) Cho, M.; Yu, J.-Y.; Nagasawa, Y.; Passino, S. A.; Fleming, G. R. *J. Phys. Chem.* **1996**, *100*, 11944−11953.
(18) de Boeij, W.; Pshenichnikov, M. S.; Wiersma, D. A. *Chem. Phys. Lett.* **1996**, *253*, 53−60.
(19) Fleming, G. R.; Cho, M. *Annu. Rev. Phys. Chem.* **1996**, *47*, 109−134.
(20) Passino, S. A.; Nagasawa, Y.; Joo, T.; Fleming, G. R. Manuscript in preparation.
(21) Joo, T.; Jia, J.; Yu, J.-Y.; Jonas, D. M.; Fleming, G. R. *J. Phys. Chem.* **1996**, *100*, 2399−2409.
(22) Joo, T.; Jia, Y.; Yu, J.-Y.; Lang, M. J.; Fleming, G. R. *J. Chem. Phys.* **1996**, *104*, 6089−6107.
(23) de Boeij, W. P.; Pshenichnikov, M. S.; Wiersma, D. A. *Chem. Phys. Lett.* **1995**, *238*, 1−8.
(24) Joo, T.; Jia, Y.; Fleming, G. R. *J. Chem. Phys.* **1995**, *102*, 4063−4068.
(25) Pshenichnikov, M. S.; Duppen, K.; Wiersma, D. A. *Phys. Rev. Lett.* **1995**, *74*, 674−677.
(26) Vöhringer, P.; Arnett, D. C.; Yang, T.-S.; Scherer, N. F. *Chem. Phys. Lett.* **1995**, *237*, 387−398.
(27) Vöhringer, P.; Arnett, D.; Westervelt, R.; Feldstein, M.; Scherer, N. F. *J. Chem. Phys.* **1995**, *102*, 4027−4036.
(28) Yang, T.-S.; Vöhringer, P.; Arnett, D. C.; Scherer, N. F. *J. Chem. Phys.* **1995**, *103*, 8346−8359.
(29) de Boeij, W. P.; Pshenichnikov, M. S.; Duppen, K.; Wiersma, D. A. *Chem. Phys. Lett.* **1994**, *224*, 243.
(30) Joo, T.; Albrecht, A. C. *Chem. Phys.* **1993**, *176*, 233−247.
(31) Bigot, J.-Y.; Portella, M. T.; Schoenlein, R. W.; Bardeen, C. J.; Migus, A.; Shank, C. V. *Phys. Rev. Lett.* **1991**, *66*, 1138−1141.
(32) Nibbering, E. T. J.; Wiersma, D. A.; Duppen, K. *Phys. Rev. Lett.* **1991**, *66*, 2464−2467.
(33) Stratt, R. M. *Acc. Chem. Res.* **1995**, *28*, 201−207.
(34) Stratt, R. M.; Cho, M. *J. Chem. Phys.* **1994**, *100*, 6700−6708.
(35) Raineri, F. O.; Resat, H.; Perng, B.-C.; Hirata, F.; Friedman, H. L. *J. Chem. Phys.* **1994**, *100*, 1477−1491.
(36) Cho, M.; Fleming, G. R.; Saito, S.; Ohmine, I.; Stratt, R. M. *J. Chem. Phys.* **1994**, *100*, 6672−6683.
(37) Roy, S.; Bagchi, B. *J. Chem. Phys.* **1993**, *99*, 9938−9943.
(38) Bagchi, B.; Chandra, A. *Adv. Chem. Phys.* **1991**, *80*, 1−126.
(39) Ladanyi, B. M.; Stratt, R. M. *J. Phys. Chem.* **1996**, *100*, 1266−1282.
(40) Mukamel, S. *Principles of Nonlinear Optical Spectroscopy*; Oxford University Press: New York, 1995.
(41) Ladanyi, B. M.; Stratt, R. M. *J. Phys. Chem.* **1995**, *99*, 2502−2511.
(42) Tanimura, Y.; Mukamel, S. *Phys. Rev. E* **1993**, *47*, 118−136.
(43) Silbey, R.; Harris, R. *J. Phys. Chem.* **1989**, *93*, 7062−7071.
(44) Calderia, A. O.; Legget, A. J. *Ann. Phys.* **1983**, *149*, 372−456.
(45) Zwanzig, R. *J. Stat. Phys.* **1973**, *9*, 215−220.
(46) Ullersma, P. *Physica* **1966**, *32*, 27−55.
(47) Ford, G. W.; Kac, M.; Mazur, P. *J. Math. Phys.* **1965**, *6*, 504−515.
(48) Ladanyi, B. M.; Klein, S. J. *J. Chem. Phys.* **1996**, *105*, 1−10.
(49) Schvaneveldt, S. J.; Loring, R. F. *J. Chem. Phys.* **1995**, *102*, 2326.
(50) Keyes, T. *J. Chem. Phys.* **1994**, *101*, 5081.
(51) Maeda, M. *Laser Dyes*; Academic Press: Tokyo, 1984.
(52) Vitale, M.; Gustafson, T. G. Personal communication.
(53) Leo, K.; Wegener, M.; Shah, J.; Chemla, D. S.; Goebel, E. O.; Damen, T. C.; Schimitt-Rink, S.; Schaefer, W. *Phys. Rev. Lett.* **1990**, *65*, 1340.
(54) van Burgel, M.; Wiersma, D. A.; Duppen, K. *J. Chem. Phys.* **1995**, *102*, 20.
(55) Vöhringer, P.; Scherer, N. F. *J. Phys. Chem.* **1995**, *99*, 2684−2695.
(56) Chang, Y. J.; Castner, E. W. J. *J. Chem. Phys.* **1993**, *99*, 113−125.
(57) Ladanyi, B. M.; Skaf, M. S. *Annu. Rev. Phys. Chem.* **1993**, *44*, 335−368.
(58) Carter, E. A.; Hynes, J. T. *J. Chem. Phys.* **1991**, *94*, 5961.
(59) Kumar, P. V.; Maroncelli, M. *J. Chem. Phys* **1991**, *103*, 3038−3060.
(60) Maroncelli, M. *J. Chem. Phys.* **1991**, *94*, 2084−2109.
(61) This result is obtained from eq 9 and eqs 2.12 and 2.14 in ref 41.
(62) Lund, P.-A.; Faurskov Nielsen, O.; Praestgaard, E. *Chem. Phys.* **1978**, *28*, 167−173.